Learning Control of Quantum Systems Using Frequency-Domain Optimization Algorithms

Daoyi Dong, *Senior Member, IEEE*, Chuan-Cun Shu, Jiangchao Chen, Xi Xing, Hailan Ma, *Graduate Student Member, IEEE*, Yu Guo, and Herschel Rabitz

***Abstract*—We investigate two classes of quantum control problems by using frequency-domain optimization algorithms in the context of ultrafast laser control of quantum systems. In the first class of problems, the system model is known and a frequency-domain gradient-based optimization algorithm is applied for searching an optimal control field to selectively and robustly manipulate the population transfer in atomic rubidium. The other class of quantum control problems involves an experimental system with an unknown model. In this case, we introduce a differential evolution algorithm with a mixed strategy to search for optimal control fields and demonstrate the capability in an ultrafast laser control experiment for the fragmentation of $Pr(hfac)_3$ molecules.**

***Index Terms*—Femtosecond laser, frequency-domain optimization, learning control, quantum control, quantum control experiment.**

I. Introduction

CONTROLLING quantum systems has become an important goal in various emerging areas including photophysics, photochemistry, quantum information, and quantum computing [1]–[5]. A number of control methods including Lyapunov control methodology [6], optimal control theory [1], robust control techniques [7]–[9], and learning control algorithms [2], [10] have been proposed to achieve various quantum control goals. Here, we focus on quantum optimal control problems where the goal is to design an optimal control field for a quantum system to achieve a given target. Optimal control theory can be developed to solve this class of quantum control problems. A limitation is that analytical optimal fields can usually be obtained only for low-dimensional quantum systems or simple control tasks. Hence, numerical optimization algorithms find wide applications to search for an optimal (usually suboptimal) field for many quantum control problems [11]. In the simulations, the commonly used optimization algorithms are usually performed in the time domain. The application of these algorithms in experiments may become challenging for the use of ultrafast laser pulses with the duration in femtosecond (fs) (1 fs $= 10^{-15}$ s) [12] and attosecond (as) (1 as $= 10^{-18}$ s) [13], [14] regimes, which cannot be directly modulated in the time domain. Experimentally, the current pulse shaping technique allows us to shape the temporal field of an ultrafast pulse [15] by modulating its spectral phase and/or amplitude in the frequency domain. This work will demonstrate how frequency-domain optimization algorithms can be employed in the numerical simulations and real experiments to search a temporally shaped ultrafast laser pulse for achieving given quantum control tasks.

For the simulations, we introduce a frequency-domain optimal control method developed recently in [16]–[18], which is able to directly calculate the optimized spectral amplitude or phase of an ultrafast laser pulse in the frequency domain while taking into account multiple constraints on the control fields. As compared with previous works [16]–[18], here we focus more on introducing the systematic frequency-domain optimal control method and present more technical details of how to develop this method. We employ the method to perform the spectral-phase-only optimization for a three-level rubidium (Rb) atom and show how the optimal spectral phase of an ultrafast laser pulse can selectively and robustly control quantum state transfer to a desired electronic level, which was not discussed previously.

For the experiments, we consider another class of quantum control problems with unknown Hamiltonians (e.g., either for complex systems or when the systems are subject to uncertainties). Due to the lack of system model information, it is usually difficult to calculate the gradient of the objective with respect to the control fields, which is crucial in the gradient-based optimization algorithm. To that end, we introduce a frequency-domain differential evolution (DE) algorithm [19] for fragmentation control of $Pr(hfac)_3$ molecules. DE [20] has shown outstanding capability to search

Manuscript received June 18, 2020; accepted August 18, 2020. Date of publication September 2, 2020; date of current version June 10, 2021. Manuscript received in final form August 19, 2020. This work was supported in part by the Australian Research Council's Discovery Projects under Project DP190101566; in part by the National Natural Science Foundation of China under Grant 61828303 and Grant 61973317, in part by NSF under Grant CHE-1464569, in part by Army Research Office (ARO) under Grant W911NF-16-1-0014, in part by the U.S. Office of Naval Research Global under Grant N62909-19-1-2129, and in part the Alexander von Humboldt Foundation of Germany. Recommended by Associate Editor J.-S. Li. *(Corresponding author: Chuan-Cun Shu.)*

Daoyi Dong is with the School of Engineering and Information Technology, University of New South Wales, Canberra, ACT 2600, Australia, and also with the Department of Chemistry, Princeton University, Princeton, NJ 08544 USA (e-mail: daoyidong@gmail.com).

Chuan-Cun Shu is with the Hunan Key Laboratory of Super-Microstructure and Ultrafast Process, School of Physics and Electronics, Central South University, Changsha 410083, China, and also with the School of Engineering and Information Technology, University of New South Wales, Canberra, ACT 2600, Australia (e-mail: cc.shu@csu.edu.cn).

Jiangchao Chen, Xi Xing, and Herschel Rabitz are with the Department of Chemistry, Princeton University, Princeton, NJ 08544 USA (e-mail: jtc5@princeton.edu; xxing@princeton.edu; hrabitz@princeton.edu).

Hailan Ma is with the School of Engineering and Information Technology, University of New South Wales, Canberra, ACT 2600, Australia (e-mail: hailan.ma@adfa.edu.au).

Yu Guo is with the Hunan Provincial Key Laboratory of Flexible Electronic Materials Genome Engineering, School of Physics and Electronic Science, Changsha University of Science and Technology, Changsha 410114, China (e-mail: guoyu@csust.edu.cn).

Color versions of one or more of the figures in this article are available online at https://ieeexplore.ieee.org.

Digital Object Identifier 10.1109/TCST.2020.3018500

for optimal solutions of various complex quantum control problems [21]–[23]. Recently, Dong et al. [19] developed a mixed-strategy-based DE algorithm (referred to as MS_DE) to search for robust control fields in both the time domain and the frequency domain [19], [25]. In this brief, we experimentally demonstrate the MS_DE algorithm for controlling the branching ratio of PrO^+/PrF^+ in the photodissociation of $Pr(hfac)_3$ molecules. Although this brief uses a similar algorithm to [19], here we aim to demonstrate optimal control of PrO^+/PrF^+ arising from $Pr(hfac)_3$ using trained intense and ultrashort femtosecond laser pulses via an MS_DE algorithm, while the experimental results in [19] focused on achieving robust control of CH_2Br^+/CH_2I^+ from CH_2BrI molecules via a multiple-sample-based MS_DE algorithm.

The brief is organized as follows. Section II provides a detailed introduction to the gradient-based optimization algorithm in the frequency domain. The application of the gradient-based optimization algorithm to selective control of quantum state transfer in a three-level Rb atom is demonstrated in Section III. In Section IV, we demonstrate the experimental results on fragmentation control of $Pr(hfac)_3$ molecules using trained femtosecond laser pulses via an MS_DE algorithm. Concluding remarks are given in Section V.

II. Gradient Algorithm for Learning Control of Quantum Systems

In this section, we assume that the model of a quantum system under consideration is known. Consider an N-level quantum system and the dynamical evolution of its state $|\psi(t)\rangle$ can be described by the Schrödinger equation

$$i\hbar\frac{d}{dt}|\psi(t)\rangle = \hat{H}(t)|\psi(t)\rangle \tag{1}$$

where $i = \sqrt{-1}$, $\hbar$ is the reduced Planck constant, $|\psi(t)\rangle$ is a complex-valued vector (expressed in Dirac notation) in an underlying Hilbert space, and $\hat{H}(t)$ is the system Hamiltonian. In the dipole approximation, the system Hamiltonian $\hat{H}(t)$ with the control field $\mathbf{u}(t)$ can be written as

$$\hat{H}(t) = \hat{H}_0 - \hat{\mu}\cdot\mathbf{u}(t) \tag{2}$$

where $\hat{H}_0$ is the free Hamiltonian and $\hat{\mu}$ is the dipole operator. We assume that the eigenvalues of $\hat{H}_0$ are E_n $(n = 1, 2, \ldots, N)$ and the corresponding eigenvectors are $|n\rangle$

$$\hat{H}_0 = \sum_{n=1}^{N} E_n|n\rangle\langle n| \tag{3}$$

where $\langle n|$ is the complex conjugate and transpose of $|n\rangle$, i.e., $\langle n| = (|n\rangle)^\dagger$. The time-dependent evolution of the quantum system from the initial state $|\psi_0\rangle$ to $|\psi(t)\rangle$ can be described by a unitary operator $\hat{U}(t)$ with $|\psi(t)\rangle = \hat{U}(t)|\psi_0\rangle$, where $\hat{U}^\dagger\hat{U} = \hat{U}\hat{U}^\dagger = I$ with identity matrix I and $\hat{U}(0) = I$. The unitary evolution operator $\hat{U}(t)$ is governed by the Schrödinger equation

$$i\hbar\frac{d}{dt}\hat{U}(t) = \hat{H}(t)\hat{U}(t). \tag{4}$$

In the quantum control problem using ultrafast laser fields, the temporal laser field $\mathscr{E}(t)$ can be written as

$$\mathscr{E}(t) = \mathrm{Re}\left[\int_0^\infty \mathbf{E}(\omega)e^{-i\omega t}d\omega\right] \tag{5}$$

where $\mathrm{Re}(x)$ returns the real part of x, and the complex spectral field $\mathbf{E}(\omega)$ can be defined in terms of the real-valued spectral amplitude $A(\omega) \geq 0$ and real-valued spectral phase $\phi(\omega)$ as

$$\mathbf{E}(\omega) = A(\omega)e^{-i\phi(\omega)}. \tag{6}$$

The state-of-the-art ultrafast pulse shaping technology has made it possible to manipulate the spectral amplitude $A(\omega)$ and the spectral phase $\phi(\omega)$ of femtosecond laser pulses. Hence, the temporal control field $\mathscr{E}(t)$ can be designed by shaping the spectral field $\mathbf{E}(\omega)$ in the frequency domain.

To formulate our method, the control objective J associated with the expectation value of an arbitrary observable $\hat{O}$ at the end of the control with $0 \leq t \leq T$ can be expressed as

$$J(\hat{O}) = \mathrm{Tr}[\hat{U}(T)|\psi_0\rangle\langle\psi_0|\hat{U}^\dagger(T)\hat{O}] \tag{7}$$

where $\hat{O}$ is a Hermitian operator and $\mathrm{Tr}(A)$ denotes the trace of A. Now we introduce a dummy variable $s \geq 0$ to track the trajectory for optimizing the spectral field $\mathbf{E}(\omega)$. Then, the gradient of J with respect to s can be expressed as

$$g_0(s) \equiv \frac{dJ}{ds} = \int_0^\infty \frac{\delta J}{\delta\mathbf{E}(s,\omega)}\frac{\partial\mathbf{E}(s,\omega)}{\partial s}d\omega. \tag{8}$$

We aim to develop an iterative algorithm to optimize the objective function J. To maximize J, we expect $(dJ/ds) \geq 0$ during the iterative process. The condition can be satisfied in the absence of constraints by choosing

$$\frac{\partial\mathbf{E}(s,\omega)}{\partial s} = \left[\frac{\delta J}{\delta\mathbf{E}(s,\omega)}\right]^* \tag{9}$$

where a^* denotes the conjugate of a.

In practical applications, (9) may be generalized to include a set of equality constraints $f_k(\mathbf{E}(s,\omega)) = C_k$, $k = 1, \ldots, K$. During the optimization process, these constraints can be written as

$$g_l(s) \equiv \frac{df_k}{ds} = \int_0^\infty \frac{\delta f_k}{\delta\mathbf{E}(s,\omega)}\frac{\partial\mathbf{E}(s,\omega)}{\partial s}d\omega = 0. \tag{10}$$

The combined requirements in (8) and (10) can be fulfilled at the same time [18]

$$\frac{\partial\mathbf{E}(s,\omega)}{\partial s} = g_0(s)\int_0^\infty S(\omega'-\omega)\sum_{k=0}^{K}[\Gamma^{-1}]_{0k}c_k^*(s,\omega')d\omega' \tag{11}$$

where $S(\omega' - \omega)$ is the filter function for smoothing the distribution of the spectral phase [16], and $c_k(s,\omega)$ is defined by

$$c_k(s,\omega) = \begin{cases} \dfrac{\delta J}{\delta\mathbf{E}(s,\omega)}, & k = 0 \\ \dfrac{\delta f_k}{\delta\mathbf{E}(s,\omega)}, & k = 1, \ldots, K \end{cases} \tag{12}$$

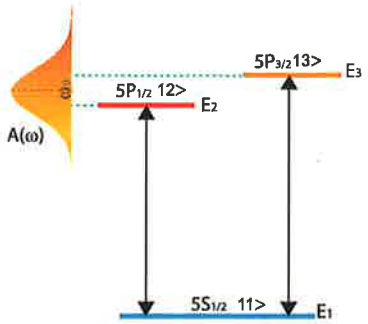

Fig. 1. Spectral phase-only control scheme in a three-level V-type Rb atom. The laser pulse with a fixed spectral amplitude $A(\omega)$ is used to excite the Rb atoms from the ground electronic state $5S_{1/2}$ to the excited electronic states $5P_{1/2}$ and $5P_{3/2}$, whose branching ratio is controlled by optimizing the spectral phase $\phi(\omega)$ of the laser pulse. In our simulations, $5S_{1/2}$, $5P_{1/2}$, and $5P_{3/2}$ are denoted by three states $|1\rangle$, $|2\rangle$, and $|3\rangle$ with energies E_1, E_2, and E_3, respectively.

and the elements of the $(K+1)\times(K+1)$ symmetric matrix Γ are given by

$$\Gamma_{kk'} = \int_0^\infty c_k(s,\omega)\int_0^\infty S(\omega'-\omega)c_{k'}^*(s,\omega')d\omega' d\omega. \quad (13)$$

In practical implementation, we can separately calculate the gradients of J with respect to $A(s,\omega)$ and $\phi(s,\omega)$. This in turn leads to two commonly used control experimental schemes, i.e., the spectral amplitude control and the spectral phase-only control. For the numerical simulations, the two control schemes can be described by

$$\frac{\delta J}{\delta A(s,\omega)} = \int_{-\infty}^{\infty}\frac{\delta J}{\delta \mathscr{E}(s,t)}\frac{\partial \mathscr{E}(s,t)}{\partial A(s,\omega)}dt \quad (14)$$

$$\frac{\delta J}{\delta \phi(s,\omega)} = \int_{-\infty}^{\infty}\frac{\delta J}{\delta \mathscr{E}(s,t)}\frac{\partial \mathscr{E}(s,t)}{\partial \phi(s,\omega)}dt. \quad (15)$$

The gradients $((\partial\mathscr{E}(s,t))/(\partial A(s,\omega)))$ and $((\partial\mathscr{E}(s,t))/(\partial\phi(s,\omega)))$ in our situation are analytically given by

$$\frac{\partial \mathscr{E}(s,t)}{\partial A(s,\omega)} = \cos[\phi(s,\omega)-i\omega t] \quad (16)$$

$$\frac{\partial \mathscr{E}(s,t)}{\partial \phi(s,\omega)} = -A(\omega)\sin[\phi(s,\omega)-i\omega t] \quad (17)$$

and the gradient $(\delta J/(\delta\mathscr{E}(s,t)))$ can be expressed as [16]

$$\frac{\delta J}{\delta \mathscr{E}(s,t)} = -2\mathrm{Im}(\mathrm{Tr}\{[\psi_0\rangle\langle\psi_0,\hat{U}^\dagger\hat{O}\hat{U}(T)]\hat{U}^\dagger\hat{\mu}\hat{U}(T)\}) \quad (18)$$

where $\mathrm{Im}(x)$ returns the imaginary part of x, and $[A,B] = AB - BA$.

III. Numerical Results on Selective Control of Atomic Rb

To illustrate the frequency-domain optimization algorithm in Section II, we consider a three-level V-type system in Fig. 1, which consists of the ground electronic state $5S_{1/2}$ and the two lowest excited electronic states $5P_{1/2}$ and $5P_{3/2}$ of a rubidium atom, denoted by $|1\rangle$, $|2\rangle$, and $|3\rangle$ with energies $E_1 = 0$, $E_2 = 12\,578.95\ \mathrm{cm}^{-1}$, and $E_3 = 12\,816.55\ \mathrm{cm}^{-1}$, respectively. The free Hamiltonian $\hat{H}_0$ is given by

$$\hat{H}_0 = \mathrm{diag}\{E_1, E_2, E_3\}. \quad (19)$$

We fix the spectral amplitude of the ultrafast laser pulse unchanged with a Gaussian distribution

$$A(\omega) = \mathscr{E}_0\frac{1}{\sqrt{2\pi}\,\Delta\omega}\exp(-(\omega-\omega_0)^2/2\Delta^2\omega)$$

with $\mathscr{E}_0 = 3.6\times10^6$ V/cm, $\omega_0 = (E_2+E_3)/2\hbar = 12\,698\ \mathrm{cm}^{-1}$ and $\Delta\omega = 177\ \mathrm{cm}^{-1}$ to excite this three-level system. The dipole moment operator $\hat{\mu}$ is given by

$$\hat{\mu} = \begin{pmatrix} 0 & \mu_{12} & \mu_{13} \\ \mu_{12} & 0 & 0 \\ \mu_{13} & 0 & 0 \end{pmatrix} \quad (20)$$

with $\mu_{12} = 2.9931$ a.u. and $\mu_{13} = 4.2275$ a.u. [27], in which the zero matrix elements imply that the transitions between $|2\rangle$ and $|3\rangle$ are forbidden.

We consider two endpoint equality constraints

$$\mathscr{E}(0) = \frac{1}{\sqrt{2\pi}}\int_{-\infty}^{\infty}A(\omega)\cos[\phi(\omega)]d\omega = 0 \quad (21)$$

and

$$\mathscr{E}(T) = \frac{1}{\sqrt{2\pi}}\int_{-\infty}^{\infty}A(\omega)\cos[\phi(\omega)-\omega T]d\omega = 0 \quad (22)$$

on the control field $\mathscr{E}(t)$, which enforce that the optimized field is turned on at $t=0$ and off at $t=T$. From (12), we derive the coefficients $c_1(s,\omega)$ and $c_2(s,\omega)$ as

$$c_1(s,\omega) = -\frac{1}{\sqrt{2\pi}}A(\omega)\sin[\phi(s,\omega)]$$

$$c_2(s,\omega) = -\frac{1}{\sqrt{2\pi}}A(\omega)\sin[\phi(s,\omega)+\omega T].$$

Furthermore, we perform an optimization procedure by shaping the spectral phase of the laser pulse while fixing the spectral amplitude. The optimization algorithm is listed in Algorithm 1.

Algorithm 1 Algorithmic Description of Gradient Algorithm

1: Solve (4) using an initial field $\mathscr{E}(s_0,t)$ with a guess of the spectral phase $\phi(s_0,\omega)$;
2: Calculate $\frac{\delta J}{\delta\phi(s_0,\omega)}$;
3: Solve the first-order differential equation (11) to obtain the first updated spectral phase $\phi(s_1 = s_0+\delta s,\omega) = \phi(s_0,\omega)+\delta s\frac{\partial\phi(s_0,\omega)}{\partial s}$;
4: Repeat Step 1 through Step 3 with the updated spectral phase as the initial guess until the "best" spectral phase is found.

We first consider a zero-flat spectral phase of $\phi(\omega)$ while leaving the spectral amplitude $A(\omega)$ unchanged, which corresponds to a transform-limited pulse

$$\mathscr{E}(s_0,t) = \mathscr{E}_0\exp\left(-t^2/2\tau_0^2\right)\cos\omega_0 t$$

with a duration of $\tau_0 = 1/\Delta\omega = 30$ fs. Fig. 2 shows the time-dependent evolution of the quantum state transfer

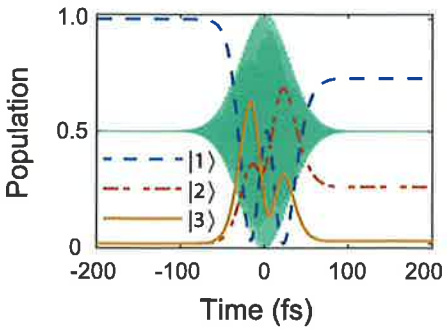

Fig. 2. Time-dependent population transfer among three states $|1\rangle$, $|2\rangle$, and $|3\rangle$ with a transform-limited pulse in green.

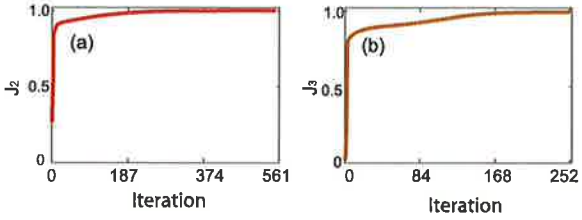

Fig. 3. Control objectives (a) $J_2 = |\langle 2|\psi(T)|^2$ and (b) $J_3 = |\langle 3|\psi(T)|^2$ versus iterations with $\sigma = 50^{-1}$.

among the three levels. Some oscillations between levels in the population transfer take place. After the pulse is off at $T = 200$ fs, all three levels are populated. In the following simulations, we selectively maximize quantum state transfer to either state $|2\rangle$ or state $|3\rangle$ by optimizing the spectral phase $\phi(\omega)$ of the laser pulse under two endpoint equality constraints by (21) and (22) while keeping its spectral amplitude $A(\omega)$ unchanged.

To achieve the goal, we define the observable $O = |j\rangle\langle j|$ with $j = 2$ or 3 to maximize the quantum state transfer to $|2\rangle$ or $|3\rangle$, respectively. We start with $\mathscr{E}(s_0, t)$ as the initial guess and take a normalized Gaussian function of the form

$$S(\omega' - \omega) = \exp(-4 \ln 2(\omega - \omega')^2/\sigma^2)$$

with a filter parameter σ. Since the speed of convergence and the shape of the optimized spectral phase are highly dependent on the choice of stepsize δs and the parameter of σ in the filter function S, we examine two different cases with a small value of $\sigma = 50$ cm^{-1} and a large value of $\sigma = 5000$ cm^{-1} and ds is varied adaptively during the iterations. Fig. 3 shows the control objectives $J_2 = |\langle 2|\psi(T)|^2$ and $J_3 = |\langle 3|\psi(T)|^2$ as a function of iterations with a small value of $\sigma = 50$ cm^{-1}. After a few hundred iterations, both objectives can monotonically increase to a very high fidelity of >0.9999 by only optimizing the spectral phase. As a result, it is possible to selectively control the population transfer to the excited electronic states $|2\rangle$ and $|3\rangle$. Fig. 4 shows the time-dependent populations with the optimized control fields and the corresponding optimized spectral phases. We can see that the populations are successfully transferred from the initial state to the target state, whereas another state is significantly populated during the transfer process, as shown

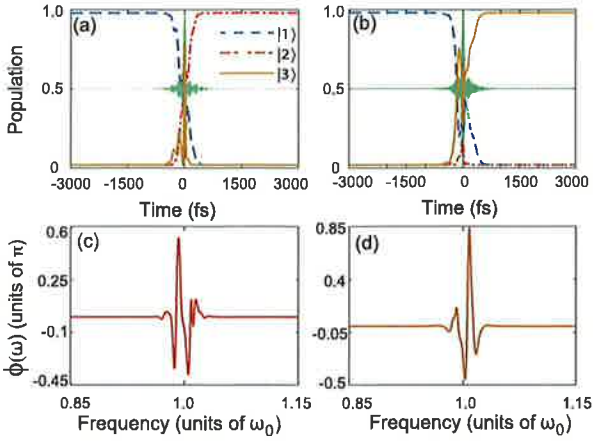

Fig. 4. Optimal population evolutions and spectral phases with $\sigma = 50$ cm^{-1}. The population evolutions of quantum state transfer to the target state (a) $|2\rangle$ and (b) $|3\rangle$ with laser pulses in green. The corresponding optimized spectral phases for (a) and (b) are shown in (c) and (d).

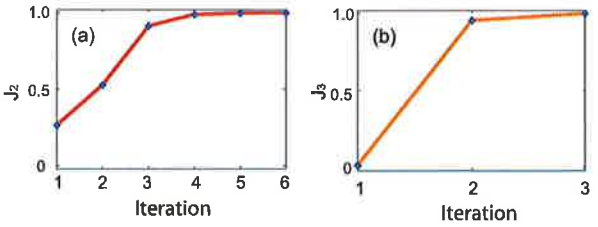

Fig. 5. Control objectives (a) $J_2 = |\langle 2|\psi(T)|^2$ and (b) $J_3 = |\langle 3|\psi(T)|^2$ versus iterations with $\sigma = 5000$ cm^{-1}.

in Fig. 4(a) and (b). The optimized spectral phases in Fig. 4(c) and (d) are complex and exhibit strong oscillations in the frequency domain. The solutions for obtaining high-fidelity quantum state transfer in such a simple quantum system are not unique. If we further decrease the value of σ in the filter S, the optimized spectral phases will become more complex than that in Fig. 4(c) and (d).

We now examine the optimization algorithm with a large value of $\sigma = 5000$ cm^{-1} and demonstrate the corresponding results in Fig. 5. It is surprising that the control objectives can rapidly and monotonically increase to a high fidelity of >0.999 after a few iterations. Fig. 6 shows the time-dependent population dynamics with the optimized fields and the corresponding optimized spectral phases. The population dynamics significantly change with the optimized fields as compared with that in Fig. 4. It is also interesting to note that the populations are successfully transferred from the initial state $|1\rangle$ to the target state $|2\rangle$ in Fig. 6(a) and $|3\rangle$ in Fig. 6(b), while the population transfer to another excited electronic state beyond the target state is clearly suppressed during the quantum state transfer process.

To gain an insight into why the population transfer to another excited electronic state beyond the target state is clearly suppressed during the quantum state transfer process in the case of $\sigma = 5000$ cm^{-1}, we first fit the optimized spectral phases in Fig. 6(c) and (d) by using a quadratic function of

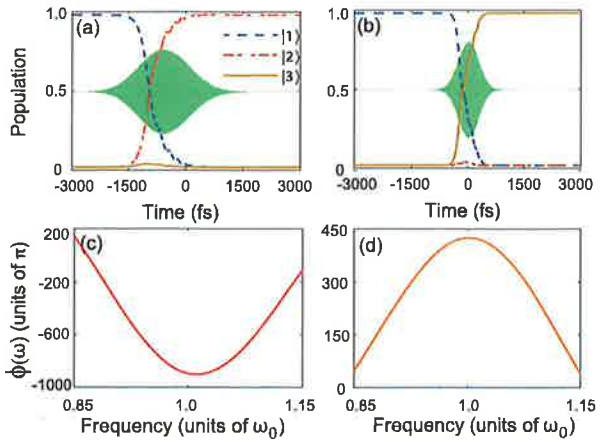

Fig. 6. Optimal population evolutions and spectral phases with $\sigma = 5000^{-1}$. The population evolutions of quantum state transfer to the target state (a) $|2\rangle$ and (b) $|3\rangle$. The corresponding optimized spectral phases for (a) and (b) are shown in (c) and (d), respectively.

$\beta_0(\omega - \omega_c)^2$ with a chirp rate β_0 and a modulated frequency ω_c. The optimized spectral phases can be fitted very well with $\beta_0 = 7191$ fs^2 and $\omega_c = 1.28423 \times 10^4$ cm^{-1} in Fig. 6(c), and with $\beta_0 = -3018$ fs^2 and $\omega_c = 1.27329 \times 10^4$ cm^{-1} in Fig. 6(d). These large chirp rates significantly prolong the optimized fields in the time domain while reducing their amplitudes as compared with the initial transform-limited pulse. The results indicate that the system is slowly guided from the initial state to the desired target state. A positively chirped pulse in Fig. 6(a) maximizes the population transfer to state $|2\rangle$ by suppressing the transfer to state $|3\rangle$, whereas a negatively chirped pulse in Fig. 6(b) leads to high efficiency of the population transfer to state $|3\rangle$ by reducing the transfer to state $|2\rangle$. It implies that an adiabatic passage is constructed between the initial and target states. Therefore, robust quantum state transfer is obtained against the variations of the system and control field. As a result, our method can provide a new approach to search for a robust control field by shaping the spectral phase of the laser pulse in the frequency domain.

Remark 1: The algorithm is also applicable for other finite-level quantum systems using phase-only control or amplitude-only control as long as we know the system model so that the gradient of a given objective function J with respect to relevant control variables can be derived in an analytical way. For many practical applications, reliable quantum system models may be unknown. In such a situation, it is not convenient to directly calculate the gradient required for the optimization algorithms. A possible strategy is that we may first identify the system model and then employ a gradient iterative algorithm to find an optimal control field. A number of identification methods has been developed to identify the reaction mechanism, system dimension, or system Hamiltonian for various quantum systems [12], [28]–[31]. However, for more complex quantum system or quantum process, it is usually difficult to identify the dynamic model before controlling it. Instead, we may employ closed-loop quantum control scheme to learn optimal ultrafast laser pulses in the frequency domain for controlling quantum systems. In the following, we will employ a DE algorithm to experimentally investigate ultrafast laser control of complex molecules Pr(hfac)$_3$.

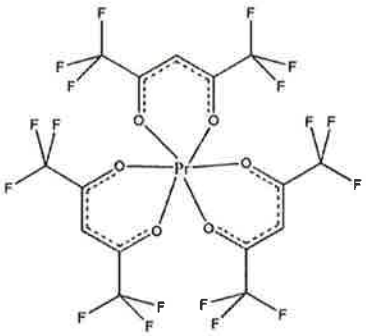

Fig. 7. Structure of a Pr(hfac)$_3$ molecule.

IV. Experimental Results on Fragmentation Control of Pr(hfac)$_3$ Using Femtosecond Laser Pulse

A. *Pr(hfac)$_3$ Molecule*

Fluorinated praseodymium complex Pr(hfac)$_3$ (hfac = hexafluoroacetylacetonate) molecules are common precursors for making thin films of praseodymium materials with metal-organic chemical vapor deposition, because of their high thermal stability and volatility [32], [33] and superior transport properties [34], [35]. The molecular structure of Pr(hfac)$_3$ is shown in Fig. 7. Even though Pr(hfac)$_3$ is an oxygen-coordinated complex, the praseodymium oxides are not easy to observe using Pr(hfac)$_3$ as a precursor in prior laser-dissociation experiments. Very small amounts of oxide fragments from Pr(hfac)$_3$ were previously reported with continuous-wave and nanosecond lasers [36]. However, Pr(hfac)$_3$ is still an excellent candidate for deposition of praseodymium fluorides [35], [37]. The formation of fluorides was explained by Talaga *et al.* [38], where they proposed a unimolecular reaction that was initiated by rotation of the $C_\alpha - C(O)$ bond bringing the CF_3 group into proximity to the metal.

Using intense and ultrashort femtosecond laser pulses, it is possible to observe a strong PrO^+ peak with the precursor Pr(hfac)$_3$ [39]. The shaped laser pulses on the fs timescale greatly restrict the $C_\alpha - C(O)$ bond rotation and enhance PrO^+ generation. The results explain why PrO^+ was rarely observed under continuous-wave and nanosecond laser beams in previous studies. The purity of the thin praseodymium oxides film and the efficiency to generate oxides are two interesting and valuable problems. Finding the best shaped pulses to optimize the PrO^+/PrF^+ ratio is a challenging task. Since we do not know the system model to describe the chemical reaction of Pr(hfac)$_3$ molecules with fs laser pulses, we employ an MS_DE algorithm (which will be discussed in Section IV-B) to find an optimal field to control the PrO^+/PrF^+ fragmentation ratio in Pr(hfac)$_3$ molecules.

B. DE With Mixed Strategies

DE is a simple but powerful stochastic search technique with wide applications [20], [40]. In DE, a population is composed of a group of individual trial solutions or *parameter vectors*, usually represented as a real-valued vector $X = [x_1, x_2, \ldots, x_D]^T$. In the process of searching, an objective function regarding a target vector X is defined as $J(X)$. Then, the learning process works by generating variations of the individuals within the given parameter space and selecting the better member to be carried into the next generation, until the "best" individual is obtained. A DE algorithm mainly includes four steps of initialization, mutation, crossover, and selection.

We denote the population (i.e., target vector) at the current generation as $X_{i,G} = [x^1_{i,G}, \ldots, x^D_{i,G}]^T$, $i = 1, \ldots,$ NP. In this brief, we use the following four diverse candidates as our mutation strategies [25], [41].

Strategy 1: DE/rand/1

$$V_i = X_{r_1} + F \cdot (X_{r_2} - X_{r_3}). \tag{23}$$

Strategy 2: DE/rand to best/2

$$V_i = X_i + F \cdot (X_{\text{best}} - X_i) + F \cdot (X_{r_1} - X_{r_2}) + F \cdot (X_{r_3} - X_{r_4}). \tag{24}$$

Strategy 3: DE/rand/2

$$V_i = X_{r_1} + F \cdot (X_{r_2} - X_{r_3}) + F \cdot (X_{r_4} - X_{r_5}). \tag{25}$$

Strategy 4: DE/current-to-rand/1

$$V_i = X_i + K \cdot (X_{r_1} - X_i) + F \cdot (X_{r_2} - X_{r_3}). \tag{26}$$

The indices r_1, r_2, r_3, r_4, and r_5 are mutually exclusive integers randomly chosen from the range [1, NP] and all of them are different from the index i. X_{best} is the best individual vector with the best fitness in the population and F is a control parameter. We set $K = 0.5$ in this brief. The DE algorithm with mixed strategy (i.e., MS_DE algorithm) is outlined in Algorithm 2 (see [41] for more detailed discussions).

Algorithm 2 Algorithmic Description of MS_DE

```
Set the generation number G = 0
for i = 1 to NP do
    initialize X_{i,0} and obtain fitness function J(X_{i,0})
end for
Set the vector with the maximum fitness as X_{best,0}
repeat (for each generation G = 0, 1, ..., G_max)
    repeat (for each vector X_i, i = 1, 2, ..., NP)
        Set parameter F_{i,G} = Normrnd(0.5, 0.3)
        Set parameter CR_{i,G} = Normrnd(0.5, 0.1)
        while CR_{i,G} < 0 or CR_{i,G} > 1 do
            CR_{i,G} = Normrnd(0.5, 0.1)
        end while
        randomly choose a strategy from candidate pool
        obtain mutant vectors V_{i,G} according to (23)-(26)
        if stragegy ∈ {1,2,3} then
            obtain U_{i,G} = [u^1_{i,G}, ..., u^D_{i,G}]^T by letting u^j_{i,G} =
        v^j_{i,G} if rand(j) ≤ CR or j = rand(1,D), and otherwise
        letting u^j_{i,G} = x^j_{i,G}
        end if
        if strategy ∈ {4} then U_{i,G} = V_{i,G}
        end if
        if J(U_{i,G}) ≥ J(X_{i,G}) then
            X_{i,G+1} ← U_{i,G},  J(X_{i,G+1}) ← J(U_{i,G}).
        end if
        Update the best vector X_{best,G} and i ← i + 1
    until i = NP
    G ← G + 1
until G = G_max
```

C. Experimental Setup

The experiments were implemented on the femtosecond laser control system in the Department of Chemistry at Princeton University. The experimental system consists of three key components: 1) a femtosecond laser system; 2) a pulse shaper; and 3) a time-of-flight mass spectrometry (TOF-MS). The femtosecond laser system (KMlab, Dragon) consists of a Ti:sapphire oscillator and an amplifier, which produces 1 mJ and 25-fs pulses centered at 790 nm. The laser pulses from the femtosecond laser system are introduced into a pulse shaper that is equipped a programmable dual-mask liquid crystal spatial light modulator. The interaction between the spatial light modulator and the learning algorithm is accomplished by LabVIEW software. The spatial light modulator has 640 pixels with 0.2 nm/pixel resolution and can modulate amplitude and phase independently [42], [43]. Every eight adjacent pixels are bundled together to form an array of 80 "grouped pixels." Each array of 80 "grouped pixels" corresponds to a control variable, which can be used to adjust the amplitude and phase values. In these experiments, we consider two constraints: one is on the amplitude values and the other is on the phase values. We fix all the amplitude values at 1 (i.e., fixed energy) for the first constraint, that is, we employ a phase-only control strategy. For the second constraint, we consider the different range of phase values, which may correspond to a situation with magnitude constraint on the control inputs. The solid $Pr(hfac)_3$ molecule samples are heated and vaporized into the gas phase in a vacuum chamber with the pressure 1.3×10^{-7} Torr. The shaped laser pulses out of the shaper are focused into the vacuum chamber, where photoionization and photofragmentation occur for the gas-phase $Pr(hfac)_3$ molecules. The fragment ions from these gas-phase $Pr(hfac)_3$ molecules are separated with a set of ion lenses and pass through a TOF tube before being collected with a microchannel plate detector. The mass spectrometry signals are recorded with a fast oscilloscope, which accumulates 3000 laser shots in 1 s before the average signal is sent to a personal computer for further analysis. A small fraction of the beam (<5%) is separated from the main beam and focused into a DET25K Thorlab photodiode. The photodiode collects signals arising from two photon absorption for optimizing a given photofragment ratio of $Pr(hfac)_3$ molecules.

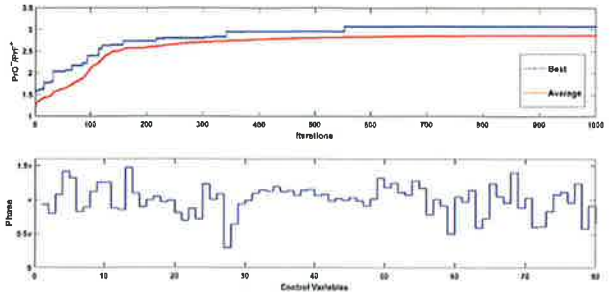

Fig. 8. Experimental result on the femtosecond laser control for optimizing the ratio between the products PrO^+ and PrF^+ using MS_DE when no constraint on the phase. (a) Ratio PrO^+/PrF^+ versus iterations, where "Best" represents the maximum fitness and "Average" represents the average fitness of all individuals during each iteration. (b) Optimized phases of 80 control variables for the optimal result that corresponds to the maximum fitness.

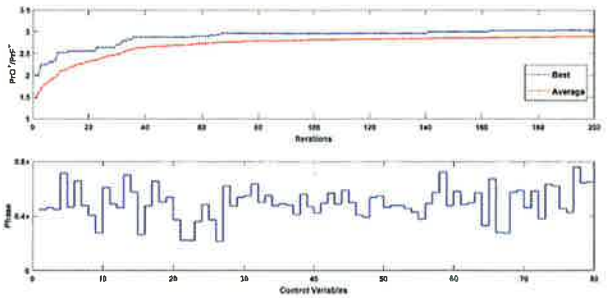

Fig. 9. Experimental result on the ratio between the products PrO^+ and PrF^+ using MS_DE when the phase is constrained in $[0, \pi]$. (a) Ratio PrO^+/PrF^+ versus iterations, where "Best" represents the maximum fitness and "Average" represents the average fitness of all individuals during each iteration. (b) Optimized phases of 80 control variables for the optimal result that corresponds to the maximum fitness.

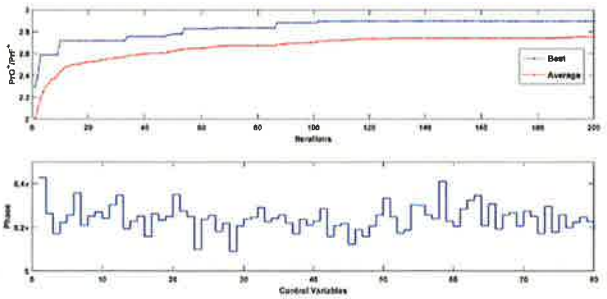

Fig. 10. Experimental result on the ratio between the products PrO^+ and PrF^+ using MS_DE when the phase is constrained in $[0, (\pi/2)]$. (a) Ratio PrO^+/PrF^+ versus iterations, where "Best" represents the maximum fitness and "Average" represents the average fitness of all individuals during each iteration. (b) Optimized phases of 80 control variables for the optimal result that corresponds to the maximum fitness.

D. Fragmentation Control

Before implementing the experiments, we need to optimize the two-photon absorption signal to identify the shortest pulse. The process can be used to remove the residual high-order dispersion in the amplifier output. The MS_DE algorithm is employed to optimize the two photon absorption signal. Then, we consider the fragmentation control of $Pr(hfac)_3$ molecules, where the fitness is defined as the photofragment ratio of PrO^+/PrF^+, i.e., $J = PrO^+/PrF^+$. We aim to maximize the objective function J. The control variables are the phases of femtosecond laser pulses and the MS_DE algorithm is employed to optimize the phases of 80 control variables. In the learning algorithm, the parameter setting is set as follows: $D = 80$ and $NP = 30$.

In the first experiment, we assume that there are no constraints on the phase values, that is, the phase values may take on arbitrary values between 0 and 2π. An experimentally acceptable termination condition of 1000 generations (iterations) is used. For 1000 iterations, it approximately takes 12 hours to run the experiment. For each generation, a total of 30 000 signal measurements are made. Fig. 8 shows the experimental results using the MS_DE algorithm, where the ratio PrO^+/PrF^+ as the fitness function is shown in Fig. 8(a) and the 80 optimized phases for the final optimal result are presented in Fig. 8(b). In Fig. 8(a), "Best" represents the maximum fitness and "Average" represents the average fitness of all individuals during each iteration. With 553 iterations, MS_DE can find an optimized pulse to make PrO^+/PrF^+ achieve 3.07. After 553 iterations, the maximum ratio remains unchanged.

In the other two experiments, we assume that the phase values can only vary between 0 and π, and between 0 and $(\pi/2)$. A termination condition of 200 generations (iterations) has been used to save the experiment time. Fig. 9 shows the results for the phase in $[0, \pi]$ from the MS_DE algorithm, where the average ratio PrO^+/PrF^+ as the fitness function is shown in Fig. 9(a) and the 80 optimized phases for the final optimal result are presented in Fig. 9(b). MS_DE can find an optimized pulse to make PrO^+/PrF^+ achieve 3.04. Even though the constraint of phase values lying only between 0 and π, the ratio PrO^+/PrF^+ can still reach 99% of the ratio in the case without phase constraint at 186 iterations. The results for the phase in $[0, (\pi/2)]$ are shown in Fig. 10. From Fig. 10(a), the MS_DE algorithm can find an optimized pulse to make PrO^+/PrF^+ achieve 2.90. From these results, it is clear that the MS_DE algorithm can assist in finding good femtosecond laser pulses to optimize the product ratio PrO^+/PrF^+ even when different constraints are placed on the amplitude and phase values of the femtosecond laser pulses.

V. Conclusion

We investigated learning control for two classes of ultrafast quantum control problems in the frequency domain where there are constraints on the control fields. When the system model is known, a frequency-domain gradient algorithm can be employed to find optimal control fields. The algorithm has been applied to atomic Rb for selective control of the population transfer. When the system model is unknown, a machine learning algorithm can be employed for searching optimal ultrafast pulses. We have experimentally implemented an MS_DE algorithm in the laboratory to control fragmentation of $Pr(hfac)_3$ molecules with different constraints on ultrafast pulses.

REFERENCES

[1] D. Dong and I. R. Petersen, "Quantum control theory and applications: A survey," *IET Control Theory Appl.*, vol. 4, no. 12, pp. 2651–2671, Dec. 2010.

[2] H. Rabitz, "Whither the future of controlling quantum phenomena?" *Science*, vol. 288, no. 5467, pp. 824–828, May 2000.

[3] H. M. Wiseman and G. J. Milburn, *Quantum Measurement and Control*. Cambridge, U.K.: Cambridge Univ. Press, 2010.

[4] M. A. Nielsen and I. L. Chuang, *Quantum Computation and Quantum Information*. Cambridge, U.K.: Cambridge Univ. Press, 2000.

[5] Y. Guo, C.-C. Shu, D. Dong, and F. Nori, "Vanishing and revival of resonance Raman scattering," *Phys. Rev. Lett.*, vol. 123, no. 22, Nov. 2019, Art. no. 223202.

[6] S. Kuang, D. Dong, and I. R. Petersen, "Rapid Lyapunov control of finite-dimensional quantum systems," *Automatica*, vol. 81, pp. 164–175, Jul. 2017.

[7] D. Dong, M. A. Mabrok, I. R. Petersen, B. Qi, C. Chen, and H. Rabitz, "Sampling-based learning control for quantum systems with uncertainties," *IEEE Trans. Control Syst. Technol.*, vol. 23, no. 6, pp. 2155–2166, Nov. 2015.

[8] J.-S. Li, J. Ruths, T.-Y. Yu, H. Arthanari, and G. Wagner, "Optimal pulse design in quantum control: A unified computational method," *Proc. Nat. Acad. Sci. USA*, vol. 108, no. 5, pp. 1879–1884, Feb. 2011.

[9] C. Chen, D. Dong, R. Long, I. R. Petersen, and H. A. Rabitz, "Sampling-based learning control of inhomogeneous quantum ensembles," *Phys. Rev. A, Gen. Phys.*, vol. 89, no. 2, Feb. 2014, Art. no. 023402.

[10] R.-B. Wu, H. Ding, D. Dong, and X. Wang, "Learning robust and high-precision quantum controls," *Phys. Rev. A, Gen. Phys.*, vol. 99, no. 4, Apr. 2019, Art. no. 042327.

[11] N. Khaneja, T. Reiss, C. Kehlet, T. Schulte-Herbrüggen, and S. J. Glaser, "Optimal control of coupled spin dynamics: Design of NMR pulse sequences by gradient ascent algorithms," *J. Magn. Reson.*, vol. 172, no. 2, pp. 296–305, Feb. 2005.

[12] C.-C. Shu, K.-J. Yuan, D. Dong, I. R. Petersen, and A. D. Bandrauk, "Identifying strong-field effects in indirect photofragmentation reactions," *J. Phys. Chem. Lett.*, vol. 8, no. 1, pp. 1–6, Jan. 2017.

[13] K.-J. Yuan, C.-C. Shu, D. Dong, and A. D. Bandrauk, "Attosecond dynamics of molecular electronic ring currents," *J. Phys. Chem. Lett.*, vol. 8, no. 10, pp. 2229–2235, May 2017.

[14] C.-C. Shu, Y. Guo, K.-J. Yuan, D. Dong, and A. D. Bandrauk, "Attosecond all-optical control and visualization of quantum interference between degenerate magnetic states by circularly polarized pulses," *Opt. Lett.*, vol. 45, no. 4, pp. 960–963, 2020.

[15] X. Xing, R. Rey-de-Castro, and H. Rabitz, "Assessment of optimal control mechanism complexity by experimental landscape hessian analysis: Fragmentation of CH_2BrI," *New J. Phys.*, vol. 16, no. 12, Dec. 2014, Art. no. 125004.

[16] C.-C. Shu, T.-S. Ho, X. Xing, and H. Rabitz, "Frequency domain quantum optimal control under multiple constraints," *Phys. Rev. A, Gen. Phys.*, vol. 93, no. 3, Mar. 2016, Art. no. 033417.

[17] C.-C. Shu, D. Dong, I. R. Petersen, and N. E. Henriksen, "Complete elimination of nonlinear light-matter interactions with broadband ultrafast laser pulses," *Phys. Rev. A, Gen. Phys.*, vol. 95, no. 3, Mar. 2017, Art. no. 033809.

[18] Y. Guo, D. Dong, and C.-C. Shu, "Optimal and robust control of quantum state transfer by shaping the spectral phase of ultrafast laser pulses," *Phys. Chem. Chem. Phys.*, vol. 20, no. 14, pp. 9498–9506, 2018.

[19] D. Dong, X. Xing, H. Ma, C. Chen, Z. Liu, and H. Rabitz, "Learning-based quantum robust control: Algorithm, applications, and experiments," *IEEE Trans. Cybern.*, vol. 50, no. 8, pp. 3581–3593, Aug. 2020.

[20] S. Das and P. N. Suganthan, "Differential evolution: A survey of the state-of-the-art," *IEEE Trans. Evol. Comput.*, vol. 15, no. 1, pp. 4–31, Feb. 2011.

[21] E. Zahedinejad, J. Ghosh, and B. C. Sanders, "High-fidelity single-shot toffoli gate via quantum control," *Phys. Rev. Lett.*, vol. 114, no. 20, May 2015, Art. no. 200502.

[22] H. Ma, C. Chen, and D. Dong, "Differential evolution with equally-mixed strategies for robust control of open quantum systems," in *Proc. IEEE Int. Conf. Syst., Man, Cybern.*, Oct. 2015, pp. 2055–2060.

[23] P. Palittapongarnpim, P. Wittek, E. Zahedinejad, S. Vedaie, and B. C. Sanders, "Learning in quantum control: High-dimensional global optimization for noisy quantum dynamics," *Neurocomputing*, vol. 268, pp. 116–126, Dec. 2017.

[24] E. Zahedinejad, J. Ghosh, and B. C. Sanders, "Designing high-fidelity single-shot three-qubit gates: A machine-learning approach," *Phys. Rev. A, Gen. Phys.*, vol. 6, no. 5, Nov. 2016, Art. no. 054005.

[25] H. Ma, D. Dong, C. C. Shu, Z. Zhu, and C. Chen, "Differential evolution with equally-mixed strategies for robust control of open quantum systems," *Control Theory Technol.*, vol. 15, no. 3, pp. 226–241, 2017.

[26] C. Wu, B. Qi, C. Chen, and D. Dong, "Robust learning control design for quantum unitary transformations," *IEEE Trans. Cybern.*, vol. 47, no. 12, pp. 4405–4417, Dec. 2017.

[27] D. A. Steck. *Rubidium 87 D Line Data*. Accessed: Nov. 25, 2019. [Online]. Available: http://steck.us/alkalidata/rubidium87numbers.pdf

[28] Y. Wang, D. Dong, B. Qi, J. Zhang, I. R. Petersen, and H. Yonezawa, "A quantum Hamiltonian identification algorithm: Computational complexity and error analysis," *IEEE Trans. Autom. Control*, vol. 63, no. 5, pp. 1388–1403, May 2018.

[29] D. Burgarth and K. Yuasa, "Quantum system identification," *Phys. Rev. Lett.*, vol. 108, no. 8, 2012, Art. no. 080502.

[30] A. Sone and P. Cappellaro, "Exact dimension estimation of interacting qubit systems assisted by a single quantum probe," *Phys. Rev. A, Gen. Phys.*, vol. 96, no. 6, Dec. 2017, Art. no. 062334.

[31] Y. Wang, D. Dong, A. Sone, I. R. Petersen, H. Yonezawa, and P. Cappellaro, "Quantum Hamiltonian identifiability via a similarity transformation approach and beyond," 2018, *arXiv:1809.02965*. [Online]. Available: http://arxiv.org/abs/1809.02965

[32] M. F. Richardson, W. F. Wagner, and D. E. Sands, "Rare-Earth trishexafluoroacetylacetonates and related compounds," *J. Inorganic Nucl. Chem.*, vol. 30, no. 5, pp. 1275–1289, Jun. 1968.

[33] C. S. Springer, D. W. Meek, and R. E. Sievers, "Rare Earth chelates of 1,1,1,2,2,3,3-heptafluoro-7,7-dimethyl-4,6-octanedione," *Inorganic Chem.*, vol. 6, no. 6, pp. 1105–1110, Jun. 1967.

[34] K. D. Pollard, H. A. Jenkins, and R. J. Puddephatt, "Chemical vapor deposition of cerium oxide using the precursors $[Ce(hfac)_3(glyme)]$," *Chem. Mater.*, vol. 12, no. 3, pp. 701–710, Mar. 2000.

[35] G. Malandrino, O. Incontro, F. Castelli, I. L. Fragala, and C. Benelli, "Synthesis, characterization, and mass-transport properties of two novel Gadolinium(III) Hexafluoroacetylacetonate polyether adducts: Promising precursors for MOCVD of GdF_3 films," *Chem. Mater.*, vol. 8, pp. 1292–1297, 1996.

[36] Q. Meng, R. J. Witte, P. S. May, and M. T. Berry, "Photodissociation and photoionization mechanisms in lanthanide-based fluorinated β-diketonate metal–organic chemical-vapor deposition precursors," *Chem. Mater.*, vol. 21, no. 24, pp. 5801–5808, Dec. 2009.

[37] G. Malandrino and I. L. Fragala, "Lanthanide 'second-generation' precursors for MOCVD applications: Effects of the metal ionic radius and polyether length on coordination spheres and mass-transport properties," *Coordination Chem. Rev.*, vol. 250, nos. 11–12, pp. 1605–1620, Jun. 2006.

[38] D. S. Talaga, S. D. Hanna, and J. I. Zink, "Luminescent photofragments of (1,1,1,5,5,5-Hexafluoro-2,4-pentanedionato) metal complexes in the gas phase," *Inorganic Chem.*, vol. 37, no. 12, pp. 2880–2887, Jun. 1998.

[39] J. Chen, X. Xing, R. Rey-de-Castro, and H. Rabitz, "Ultrafast photofragmentation of $Ln(hfac)_3$ with a proposed mechanism for forming high mass fluorinated products," *Sci. Rep.*, vol. 10, no. 1, p. 7066, Dec. 2020.

[40] R. Storn and K. Price, "Differential evolution-a simple and efficient heuristic for global optimization over continuous spaces," *J. Global Optim.*, vol. 11, no. 4, pp. 341–359, 1997.

[41] D. Dong *et al.*, "Learning control of quantum systems using frequency-domain optimization algorithms," 2020, *arXiv:2005.13080*. [Online]. Available: http://arxiv.org/abs/2005.13080

[42] K. M. Tibbetts, X. Xing, and H. Rabitz, "Systematic trends in photonic reagent induced reactions in a homologous chemical family," *J. Phys. Chem. A*, vol. 117, pp. 8025–8215, 2013.

[43] K. M. Tibbetts, X. Xing, and H. Rabitz, "Optimal control of molecular fragmentation with homologous families of photonic reagents and chemical substrates," *Phys. Chem. Chem. Phys.*, vol. 15, pp. 18012–18022, 2013.